# Supplementary Information: Maxwell's Equations with a Measurement-Dependent Collapsible Field

**Abstract**

Classical electrodynamics presumes that all physically relevant field degrees of freedom are directly accessible to measurement. We examine whether coherence-dependent dynamics can nevertheless influence observable behaviour while remaining operationally hidden. We introduce a minimal extension of Maxwell's equations incorporating a hidden field whose influence is transient and suppressed by measurement-like collapse. The field neither sources spacetime curvature nor introduces new interactions, but modifies electromagnetic propagation and energy redistribution in a coherence-limited regime. Analytical derivations and numerical simulations demonstrate transient phase accumulation, energy-density gradients, and short-lived force-like responses that vanish smoothly as the collapse rate increases, recovering standard electrodynamics. The resulting dynamics exhibit a source–mediator–sink structure governed by collapse control. We identify experimentally accessible signatures based on dispersive, phase-sensitive measurements, establishing a controlled framework for probing hidden coherence effects within classical field theory.

# Supplementary Note 1 — Derivation of the Euler–Lagrange equation

We derive the equation of motion for the modified electromagnetic field starting from the one–dimensional Lagrangian density

$$\mathcal{L}(x,t) = \frac{1}{2}\left(\frac{\partial E_{\mathrm{mod}}}{\partial t}\right)^2 - \frac{1}{2}\left(\frac{\partial E_{\mathrm{mod}}}{\partial x}\right)^2 - V(C), \tag{1}$$

where

$$E_{\mathrm{mod}}(x,t) = E_0(x,t) + \lambda\, C(x,t), \qquad V(C) = \tfrac{1}{2}M^2C^2. \tag{2}$$

The modified electric field $E_{\mathrm{mod}}(x,t)$ is treated as the dynamical variable, while $C(x,t)$ is regarded as an auxiliary field with externally prescribed collapse dynamics.

The Euler–Lagrange equation for a scalar field in one spatial dimension is linear and second order:

$$\frac{\partial}{\partial t}\left(\frac{\partial \mathcal{L}}{\partial(\partial_t E_{\mathrm{mod}})}\right) + \frac{\partial}{\partial x}\left(\frac{\partial \mathcal{L}}{\partial(\partial_x E_{\mathrm{mod}})}\right) - \frac{\partial \mathcal{L}}{\partial E_{\mathrm{mod}}} = 0. \tag{3}$$

Nonlinearity only arises if $C$ depends on $E_0$, effectively providing feedback. Evaluating termwise,

$$\frac{\partial \mathcal{L}}{\partial(\partial_t E_{\mathrm{mod}})} = \partial_t E_{\mathrm{mod}}, \qquad \frac{\partial}{\partial t}\left(\partial_t E_{\mathrm{mod}}\right) = \partial_t^2 E_{\mathrm{mod}}, \tag{4}$$

$$\frac{\partial \mathcal{L}}{\partial(\partial_x E_{\mathrm{mod}})} = -\,\partial_x E_{\mathrm{mod}}, \qquad \frac{\partial}{\partial x}\left(-\,\partial_x E_{\mathrm{mod}}\right) = -\,\partial_x^2 E_{\mathrm{mod}}. \tag{5}$$

Since the Lagrangian has no explicit dependence on $E_{\mathrm{mod}}$ itself,

$$\frac{\partial \mathcal{L}}{\partial E_{\mathrm{mod}}} = 0. \tag{6}$$

Substituting into the Euler-Lagrange equation yields

$$\partial_t^2 E_{\mathrm{mod}} - \partial_x^2 E_{\mathrm{mod}} = 0. \tag{7}$$

Expressing this in terms of the background and hidden fields gives

$$\partial_t^2 (E_0 + \lambda C) - \partial_x^2 (E_0 + \lambda C) = 0, \tag{8}$$

or equivalently,

$$\left(\partial_t^2 - \partial_x^2\right) E_0 = -\,\lambda \left(\partial_t^2 - \partial_x^2\right) C. \tag{9}$$

This form explicitly shows that the hidden field enters the electromagnetic dynamics as an effective source term. As $C(x,t)$ collapses in time, this source vanishes, and the standard one–dimensional wave equation for the classical field $E_0(x,t)$ is recovered.

# Supplementary Note 2 — Dynamical structure and possible extensions

The Euler–Lagrange equation obtained from the present formulation is second–order in space and time, ensuring wave–like propagation and supporting rich transient dynamics driven by the presence of the collapsible field. In its current form, however, the equation remains linear in the modified electromagnetic field, with nontrivial behavior arising from time–dependent forcing rather than intrinsic nonlinearity. The linear coupling,

$$E_{\mathrm{mod}} = E_0 + \lambda C,$$

acts to reshape electromagnetic propagation without introducing a direct force, thereby modifying the effective dynamical environment experienced by the field. The collapse parameter $M$ enters through the quadratic potential,

$$V(C) = \frac{1}{2} M^2 C^2,$$

which imposes an energetic penalty on sustained hidden–field configurations and ensures their suppression over time. Larger values of $M$ correspond to more rapid collapse and a faster return to classical electromagnetic behavior, providing a simple phenomenological analogue of measurement–induced decoherence. A natural extension of the model is to promote the hidden field to a fully dynamical degree of freedom that responds to the electromagnetic state, thereby introducing genuine nonlinearity and feedback. One representative example is an evolution equation of the form

$$\partial_t^2 C - \partial_x^2 C + M^2 C = \alpha E_{\text{mod}}^2,$$

which would allow electromagnetic excitations to influence the persistence and collapse of the hidden field. Alternatively, nonlinear interaction terms may be introduced directly at the level of the Lagrangian, such as

$$\mathcal{L}_{\text{int}} = \lambda \, C \, E^2,$$

coupling the hidden field to the local electromagnetic energy density while preserving the collapse mechanism enforced by the quadratic potential. These extensions provide a controlled pathway toward emergent behavior, including state–dependent dynamics and coherence–driven effects, while remaining compatible with the interpretation of the collapsible field as a transient mediator rather than a source of fundamental spacetime curvature.

# Supplementary Note 3 — Phase accumulation due to hidden-field

## Experimental hypothesis

Phase accumulation may be a relevant addition to force- and trajectory-based experimental diagnostic probe of the hidden, collapsible field. This because phase is an ideal observable in this context since it can be accessed using weak or dispersive techniques, such as interferometry or cavity phase readout, without strongly localizing the field or inducing collapse. We suggest a *cryogenic superconducting cavity* as the experimental platform. Our approach is to neither invoke forces or spacetime curvature, nor require force measurements or gravitational analogies. For small $M$, coherent phase builds up over extended times, while increasing $M$ progressively suppresses phase accumulation and restores the classical limit.

## Hidden-field contribution to phase

We consider a time-dependent hidden field of the form

$$C(t) = C_0 \, \mathrm{e}^{-Mt} \cos(\omega t), \tag{10}$$

where $M$ is the collapse (measurement-like) rate and $\omega$ sets the characteristic oscillation frequency. The parameter $C_0$ denotes the initial coherence amplitude. The observable EM field couples linearly to $C(t)$ with strength $\lambda$, such that the hidden field contributes an additional phase offset to a probe field. The accumulated phase over an observation window $[0, T]$ is then given by

$$\Delta\phi(M, T) = \lambda \int_0^T C(t) \, \mathrm{d}t = \lambda C_0 \int_0^T \mathrm{e}^{-Mt} \cos(\omega t) \, \mathrm{d}t. \tag{11}$$

The integral can be evaluated analytically as

$$\Delta\phi(M,T) = \lambda C_0 \frac{M\left[1 - \mathrm{e}^{-MT}\cos(\omega T)\right] + \omega\,\mathrm{e}^{-MT}\sin(\omega T)}{M^2 + \omega^2}, \tag{12}$$

which highlights the competing roles of oscillatory coherence ($\omega$) and collapse ($M$).

## Interpretation of simulation

Fig. S1(a) illustrates how the accumulated phase ($\Delta\phi$) changes over time for different values of the collapse rate, $M$. The y-axis represents a cumulative effect, or an 'accumulated phase,' ($\Delta\phi$). This is the time-integral of the collapsible field $C$, whose significance is to imply that $C$ might represent something that contributes to a phase shift or a similar cumulative effect in a system. The influence of $M$, the 'measurement-like parameter' or 'collapse rate' is as follows:

1. Lower M values (e.g., $M = 0.1$, 0.5): $\Delta\phi$ increases more significantly and over a longer duration before eventually leveling off at a higher value. This suggests that when the collapse rate is low, the collapsible field $C$ persists longer, allowing its cumulative effect to build up more.
2. Higher M values (e.g., $M = 1.0$, 2.0): $\Delta\phi$ rises less steeply and reaches a plateau much faster, at a lower overall value. This indicates that a higher collapse rate M causes the field $C$ to decay more quickly, thereby limiting its total accumulated influence on the phase.

In summary, higher $M$ leads to a weaker and shorter-lived cumulative effect (less accumulated phase), while a lower $M$ allows for a stronger and more sustained cumulative effect. While Fig. S1(a) illustrates the time evolution of phase accumulation for different collapse rates, it is also instructive to examine directly how the accumulated phase depends on the collapse parameter at a fixed observation time. Such a representation makes explicit the collapse-controlled suppression of hidden-field influence and highlights the exponential nature of the effect. Fixing an observation time $T^*$, the accumulated phase is given by $\Delta\phi(M, T^*) = \lambda \int_0^{T^*} C_0\, e^{-Mt} \cos(\omega t)\, dt$. Fig. S1(b) plots $\Delta\phi(M, T^*)$ as a function of $M$ on a logarithmic vertical axis. For small $M$, phase accumulation remains appreciable, reflecting the persistence of hidden-field coherence over the observation window. As $M$ increases, the accumulated phase decreases approximately exponentially, indicating rapid suppression of coherent contributions. In the large-$M$ limit, $\Delta\phi$ approaches zero smoothly, demonstrating that hidden-field effects are strongly attenuated and that classical electromagnetic behavior is recovered. This

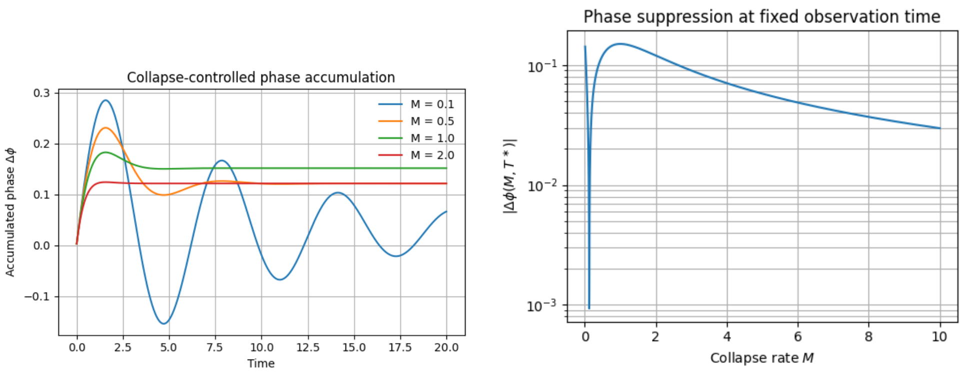


**Fig. 1** Supplementary Figure S1 — Collapse-controlled phase accumulation induced by the hidden field. **(a)** Time evolution of the accumulated phase $\Delta\phi(M, T) = \lambda \int_0^{T} C(t)\, dt$ for several values of the collapse rate $M$, with $C(t) = C_0 e^{-Mt} \cos(\omega t)$. For small $M$, coherent oscillations persist over extended durations, allowing sustained phase accumulation before saturation through destructive interference. Increasing $M$ progressively suppresses accumulation, reflecting a transition from source-like to mediator- and sink-like behavior. **(b)** Accumulated phase evaluated at a fixed observation time $T^*$, plotted as a function of $M$ on a log-linear scale. The phase decreases approximately exponentially with increasing $M$, illustrating rapid suppression of hidden-field coherence. In the large-$M$ limit, $\Delta\phi$ vanishes smoothly, demonstrating the self-terminating nature of hidden-field effects and the recovery of classical electromagnetic behavior.

log-linear representation provides a clear visualization of the coherence-limited nature of the model, showing that the collapse parameter sets a sharp but continuous boundary between regimes in which hidden-field effects are experimentally observable and those in which they are effectively erased by measurement.

# Supplementary Note 4 — Methods

Experiments are proposed using high–quality-factor superconducting microwave cavities operated at millikelvin (mK) temperatures in a dilution refrigerator. Such cavities support long-lived electromagnetic coherence while enabling phase-sensitive, dispersive readout that minimally perturbs the stored field. Multiple three-dimensional cavities fabricated from superconducting materials (e.g. Nb, Al, $Nb_3Sn$) are envisaged, with target internal quality factors exceeding $Q \sim 10^{10}$. Cavities are housed within multilayer superconducting and mu-metal magnetic shielding, and all microwave lines are heavily filtered and thermally anchored to suppress environmental noise.

## Coherent field preparation and stabilization

A phase-stable coherent microwave tone is injected into a selected cavity mode using ultra-low-noise frequency synthesis referenced to a stable clock source. Active feedback is employed to stabilize both amplitude and resonance frequency, permitting precise characterization of baseline linewidth, phase noise, and coherence time prior to data acquisition. Spatially structured standing-wave modes are selected to maximize sensitivity to coherence-dependent effects.

## Dispersive phase readout

The cavity is weakly coupled to a probe transmission line operating strictly in the dispersive regime, with an average probe photon number $\bar{n}_{\mathrm{probe}} \ll 1$. Phase and frequency shifts are monitored via homodyne or heterodyne detection without measurable photon absorption or cavity heating. Probe power is restricted to verified weak-measurement regimes to ensure that measurement back-action does not dominate the dynamics. Calibration is performed using injected synthetic phase perturbations to quantify instrumental response and residual back-action.

## Hidden-field activation protocol

Within the proposed framework, coherent cavity excitation is hypothesized to support a transient hidden-field contribution whose influence manifests indirectly through energy redistribution and phase modification of the electromagnetic mode. Rather than attempting to detect this field directly, observables such as time-dependent phase accumulation, anomalous frequency drift, or changes in effective dispersion are monitored continuously during cavity excitation and relaxation. All measurements are referenced to pre-established baselines to exclude thermal, Kerr, and technical effects.

## Mechanical coupling (optional)

To probe force-like signatures associated with hidden-field energy gradients, a nanomechanical resonator or suspended dielectric test mass may be positioned in proximity to the cavity field or integrated as a weakly coupled mechanical mode. Mechanical resonance frequency shifts or equilibrium displacements are inferred using back-action–evading measurement protocols, allowing sensitivity to effective potential gradients without localizing cavity photons. Correlation with cavity coherence, rather than probe strength, is used to discriminate candidate effects.

## Control of effective collapse rate

The effective collapse rate is treated as an externally tunable parameter controlled by probe strength, engineered cavity linewidth, or adjustable environmental coupling. Systematic variation of these parameters enables the mapping of observables as a function of collapse rate. The framework predicts sustained deviations at weak collapse and rapid suppression at strong collapse, providing a clear criterion for internal consistency and falsifiability.

## Sensitivity estimates

State-of-the-art superconducting microwave cavities permit phase sensitivities at the level of $\delta\phi \sim 10^{-6}$–$10^{-8}$ rad/$\sqrt{\mathrm{Hz}}$ under dispersive readout, corresponding to resolvable fractional frequency shifts below $10^{-12}$ over integration times of order $10^3$–$10^4$ s. For mechanical probes with effective masses in the picogram–nanogram range and quality factors $Q_m \gtrsim 10^6$, force sensitivities in the range $10^{-18}$–$10^{-20}$ N/$\sqrt{\mathrm{Hz}}$ are achievable using back-action–evading techniques. These sensitivities are sufficient to detect or tightly bound coherence-limited phase accumulation and force-like effects predicted by the model, while remaining well below thresholds associated with cavity heating or nonlinear electromagnetic response.

## Risk mitigation and systematic errors

Primary sources of systematic error include thermal drifts, residual Kerr nonlinearity, radiation-pressure back-action, vibrational coupling, and excess technical phase noise. These effects are mitigated through active temperature stabilization, operation at low photon number, independent calibration of Kerr coefficients, vibration isolation, and cross-correlation between independent detection chains. Null measurements are performed by repeating experiments in the absence of coherent cavity excitation, under deliberately strong probe conditions, and in overdamped cavity configurations. All candidate signatures must vanish continuously as the effective collapse rate is increased, providing a stringent internal consistency check.

## Analysis and reproducibility

Data analysis focuses on time-resolved phase and frequency statistics and their scaling with the collapse parameter. Bayesian model comparison is employed to distinguish candidate signals from thermal and known quantum noise sources. Absence of collapse-controlled scaling places direct upper bounds on coupling parameters. All cavity designs, calibration procedures, and raw phase and frequency data are intended for release to enable independent replication and verification.

## Supplementary Note 5 — Stepwise experimental procedure

### Conceptual definition

1. Identify primary electromagnetic observables, including phase drift, resonance frequency shift, linewidth modification, and coherence time, together with secondary mechanical observables where applicable.
2. Define null criteria requiring that all candidate signatures vanish smoothly as the effective collapse rate is increased.
3. Pre-register analysis protocols, statistical thresholds, and falsification criteria to avoid post-selection and confirmation bias.

### Infrastructure and environment

1. Install a dilution refrigerator operating at base temperatures below 10 mK with active vibration isolation.
2. Implement multilayer superconducting and mu-metal magnetic shielding to suppress external magnetic and electromagnetic noise.
3. Heavily filter and thermally anchor all microwave lines to minimize radiative heating and technical phase noise.

### Superconducting cavity fabrication and characterization

1. Fabricate interchangeable three-dimensional superconducting microwave cavities (e.g. Nb, Al, $Nb_3Sn$) targeting internal quality factors $Q > 10^{10}$.

2. Engineer spatially structured standing-wave modes to enhance sensitivity to coherence-dependent effects.
3. Characterize all cavity modes at millikelvin temperatures, establishing baseline resonance frequencies, linewidths, and phase noise spectra.

## Coherent field preparation

1. Inject a phase-stable coherent microwave tone into a selected cavity mode using ultra-low-noise signal generation.
2. Stabilize amplitude and frequency via active feedback referenced to a stable frequency standard.
3. Measure baseline coherence time and phase diffusion in the absence of probe readout.

## Dispersive weak-measurement readout

1. Weakly couple the cavity to a probe transmission line operating strictly in the dispersive regime.
2. Maintain an average probe photon number $\bar{n}_{\text{probe}} \ll 1$ to suppress measurement-induced collapse.
3. Perform homodyne or heterodyne phase-only readout and calibrate measurement back-action using injected reference phase signals.

## Hidden-field activation protocol

1. Activate coherent cavity excitation with a controlled temporal envelope.
2. Continuously monitor phase, frequency, and dispersion during excitation, steady state, and relaxation.
3. Identify transient signatures correlated with coherent excitation while excluding thermal, Kerr, and technical artifacts.

### Mechanical probe coupling

1. Introduce a nanomechanical resonator or suspended dielectric test mass weakly coupled to the cavity field.
2. Measure mechanical resonance frequency shifts or equilibrium displacements using back-action–evading protocols.
3. Verify that mechanical responses correlate with cavity coherence rather than probe intensity.

### Collapse-rate control

1. Tune the effective collapse rate by varying probe strength, engineered cavity loss, or controlled environmental coupling.
2. Map observable signatures as functions of the collapse parameter, identifying source-like, mediator-like, and sink-like regimes.

### Null tests and consistency checks

1. Repeat measurements with no cavity excitation, strong probe power, and overdamped cavity configurations.
2. Confirm that all candidate signals disappear continuously under strong collapse conditions.
3. Compare results across cavity materials, geometries, and mode structures.

### Data analysis and falsifiability

1. Extract time-resolved phase accumulation, coherence decay, and scaling behavior with the collapse rate.
2. Perform Bayesian model comparison against thermal and known quantum noise sources.

3. Interpret absence of collapse-controlled scaling as direct bounds on model parameters.

### Interpretation and dissemination

1. Report results strictly in terms of electromagnetic observables without invoking spacetime curvature or preferred frames.
2. Release cavity designs, calibration procedures, and raw data to enable independent replication.
3. Publish explicit null results and parameter bounds alongside any candidate observations.

## References


[1] Cahaya, A.B.: Zitterbewegung, momentum, and spin dynamics of electromagnetic waves in a linear dielectric medium. Physical Review A **112**(3), 033721 (2025)

[2] Li, S., Ma, Y., Yuan, F., Zhang, X.: Effective dynamics of loop quantum kaluza-klein cosmology. Physical Review D **113**(4), 041503 (2026) https://doi.org/10.1103/pv8v-wphn

[3] Heidenreich, B., Lotito, M.: Proving the weak gravity conjecture in perturbative string theory. part i. the bosonic string. Journal of High Energy Physics **2025**(5), 1–44 (2025)

[4] Li, B.: Emergent gravity and gauge interactions from a dynamical temporal field. Reports in Advances of Physical Sciences **9**, 2550017 (2025) https://doi.org/10.1142/S2424942425500173

[5] Dong, Y.-Q., Cao, Z., Liu, Y.-X.: Gravitational wave detection based on gravitomagnetic effects. Physics Letters B, 140343 (2026) https://doi.org/10.1016/j.

physletb.2026.140343

[6] Yao, S., Zhou, X., Hu, G.: Investigation of the negative-mass behaviors occurring below a cut-off frequency. New Journal of Physics **12**(10), 103025 (2010) https://doi.org/10.1088/1367-2630/12/10/103025

[7] Morgan, A.D., Boyd, M.E., Leeah, S.: Field-coupled propulsion diagnostics from energetic flow imaging: Structural analysis and resonant dynamics. Advances in Astronautics, 1–15 (2026) https://doi.org/10.1007/s42423-026-00215-8

[8] Criado, J.C., Jaeckel, J., Spannowsky, M.: Field redefinitions in classical field theory with some quantum perspectives. Physical Review D **111**(7), 076019 (2025) https://doi.org/10.1103/PhysRevD.111.076019

[9] Noel, C., Niroula, P., Zhu, D., Risinger, A., Egan, L., Biswas, D., Cetina, M., Gorshkov, A.V., Gullans, M.J., Huse, D.A., *et al.*: Measurement-induced quantum phases realized in a trapped-ion quantum computer. Nature Physics **18**(7), 760–764 (2022) https://doi.org/10.1038/s41567-022-01619-7

[10] Agrawal, U., Lopez-Piqueres, J., Vasseur, R., Gopalakrishnan, S., Potter, A.C.: Observing quantum measurement collapse as a learnability phase transition. Physical Review X **14**(4), 041012 (2024) https://doi.org/10.1103/PhysRevX.14.041012

[11] Almeida, C.R., Jacquet, M.J.: Analogue gravity and the hawking effect: historical perspective and literature review. The European Physical Journal H **48**(1), 15 (2023) https://doi.org/10.1140/epjh/s13129-023-00063-2

[12] Taylor, T.S.: A First Graduate Course in Quantum Field Theory: For Doctoral Level Physics. CRC Press, ??? (2026)

[13] Southgate, A., Oquatre-six, C.: Penrose gravity-induced collapse and empirical prospects (2026)

[14] Lee, J., Kim, J., Shim, S., Yang, Y., Choi, J., Rho, J., Lee, D., Kim, M.: Real-time observation of the spin hall effect of light using metasurface-enabled single-shot weak measurements. Nature Communications **16**(1), 2699 (2025) https://doi.org/10.1038/s41467-025-56728-7

[15] Lovett, S., Walker, P.M., Osipov, A., Yulin, A., Naik, P.U., Whittaker, C.E., Shelykh, I.A., Skolnick, M.S., Krizhanovskii, D.N.: Observation of zitterbewegung in photonic microcavities. Light: Science & Applications **12**(1), 126 (2023) https://doi.org/10.1038/s41377-023-01162-x

[16] Genovese, M.: Research on hidden variable theories: A review of recent progresses. Physics Reports **413**(6), 319–396 (2005) https://doi.org/10.1016/j.physrep.2005.03.003

[17] Mattingly, D.: Modern tests of lorentz invariance. Living Reviews in relativity **8**(1), 1–84 (2005) https://doi.org/10.12942/lrr-2005-5

[18] Mohanty, S., Panda, S., Vidyarthi, A.: Testing the starobinsky model of inflation with resonant cavities. Physical Review D **113**(6), 063574 (2026)

[19] De Amorim, R.C., Mirkin, B.: Minkowski metric, feature weighting and anomalous cluster initializing in k-means clustering. Pattern Recognition **45**(3), 1061–1075 (2012) https://doi.org/10.1016/j.patcog.2011.08.012

[20] Bassi, A., Ulbricht, H.: Collapse models: from theoretical foundations to experimental verifications. In: Journal of Physics: Conference Series, vol. 504, p. 012023 (2014). https://doi.org/10.1088/1742-6596/504/1/012023

[21] Nasser, A.D.: The quantum measurement problem: Foundations, interpretations, and recent developments (2025) https://doi.org/10.20944/preprints202504.1117.v1

[22] Finster, F., Isidro, J.M., Paganini, C.F., Singh, T.P.: Theoretically motivated dark electromagnetism as the origin of relativistic modified newtonian dynamics. Universe **10**(3), 123 (2024) https://doi.org/10.3390/universe10030123

[23] Kong, O.C.: Quantum mechanics in curved space (time) with a noncommutative geometric perspective. Chinese Journal of Physics **96**, 690–699 (2025) https://doi.org/10.1016/j.cjph.2025.05.029